Journal of Polymers and the Environment
https://doi.org/10.1007/s10924-022-02464-8

ORIGINAL PAPER

Insights into Effective Adsorption of Lead ions from Aqueous Solutions by Using Chitosan-Bentonite Composite Beads

Zeynep Mine Şenol[1] · **Selçuk Şimşek**[2]

Accepted: 20 April 2022

Abstract

The chitosan (Ch)—bentonite (B) composite was synthesized and its adsorption properties were investigated for lead ions. The characterization of the Ch-B composite was clarified by FT-IR, SEM, and pzc studies. Factors affecting Pb^{2+} ion adsorption from aqueous solution; pH, temperature, adsorbent dose, adsorbate concentration, adsorption time, and temperature were examined within the scope of the study. Adsorption was found to increase with increasing pH under acidic conditions, and the adsorbent surface was found to be positive under pH: 5.95. It was found that the adsorption isotherm was suitable for the Langmuir isotherm model and the adsorption capacity from this model was 0.425 mol kg^{-1}. It was observed that the adsorption kinetics fit the PSO and IPD models. Thermodynamic analysis of the adsorption was made and it was determined that the adsorption process was endothermic, with increasing entropy and spontaneous. The reuse conditions of the adsorbent were investigated and it was found that the adsorbed ion was recovered 84% in 0.1 M HCl.

Keywords Adsorption · Chitosan · Bentonite · Pb^{2+} · Wastewater treatment

Introduction

With the acceleration of industrialization, synthetic dyes and heavy metals among the organic pollutants mixed with the environment and wastewater pose a danger to human health and the environment [1]. Disposal of synthetic dyes and heavy metals into the environment without waste treatment poses a serious threat to human health as a result of mixing with both aquatic life and drinking water [2].

One of the heavy metals causing environmental pollution is lead. Lead is generally found in the wastewater of metal, metal plating industry, and mining activities [3]. Lead is highly toxic to human health. If the concentration of lead in the blood is above 0.4 μmol L^{-1}, it has negative effects on heme synthesis inhibition in the blood, kidney, cardiovascular system, endocrine and immune system, and blood pressure [4]. Therefore, removing lead from water is important for human health and the environment. Many physicochemical approaches have been developed for the removal of waste heavy metals and dyes [5]. In these approaches, ion exchange, reverse osmosis, precipitation, ultrafiltration, and adsorption are commonly used techniques [6]. However, most of these techniques are not preferred due to cost, difficulty in implementation, requiring advanced technology, and ineffectiveness. Among these, adsorption stands out with its cost, ease of use, and rich adsorbent options [7]. Adsorption isolates organic or inorganic compounds from the aqueous or gas phase by binding on a solid surface through covalent bonding, ion exchange, chelation, or Van der Waals interactions. It is quite common to remove heavy metals and dyes, which have a large place among the pollutants, by the adsorption method [8]. Natural rocks and minerals can be used as adsorbents, among these natural adsorbents, minerals such as bentonite, zeolite, diatomite, dolomite, and vermiculite are used by many researchers as adsorbents in the removal of heavy metal ions from aqueous solutions due to their low cost [9].

Chitosan is the most abundant natural polymer after cellulose, obtained by deacetylation of chitin. Chitosan has proven to be one of the most promising adsorbents for heavy metal removal due to its low cost, highly available,

✉ Zeynep Mine Şenol
msenol@cumhuriyet.edu.tr

✉ Selçuk Şimşek
simsek@cumhuriyet.edu.tr

[1] Department of Food Technology, Zara Vocational School, Cumhuriyet University, 58140 Sivas, Turkey

[2] Department of Chemistry, Faculty of Science, Cumhuriyet University, 58140 Sivas, Turkey

Published online: 10 May 2022

non-toxic, bioactive, biocompatible, biodegradable, and non-toxicity [10, 11]. Chitosan is used in many sectors such as textiles, cosmetics, the production of medical supplies, and agricultural areas [12]. At the same time, chitosan is widely used in the removal of various dyes and heavy metals due to the functional groups in its structure [13]. The –OH, $–NH_2$, and $–NH–CO–CH_3$ groups in the chitosan chain function as chelating agents for capturing almost all kinds of ions physically or chemically [14]. However, chitosan has disadvantages such as easy agglomeration, solubility in acid solutions, and poor strength [15]. These negative properties of chitosan are overcome by forming a composite with various natural minerals [10]. Chitosan composites have resistance to an acidic environment and a high adsorption capacity for dyes and heavy metals.

Bentoniteis a common and commercially used term for clays whose main mineral ismontmorillonite and is a soft colloidal aluminum hydrosilicate containing atleast 85% montmorillonite. Bentonite is a clay mineral that swells on contactwith water, can be activated with acid, thickens drilling mud, and displays alarge surface area. Bentonite shows very good adsorbing properties due to itshigh surface area [16]. However, bentoniteshows agglomeration in water due to its hydrophilic character. To eliminatethis negative feature of bentonite and to increase its interest in terms ofadsorption, polymer-bentonite composites are synthesized by processing withvarious polymers.

In thestudies to date, the adsorbent property of bentonite has been investigated, itscomposites have been synthesized with various polymers by different methods,but no research has been conducted on the synthesis of Ch-Bcomposite cross-linked with epichlorohydrin and tripolyphosphate. In this study, Ch-B composite beads cross-linked withepichlorohydrin and tripolyphosphate were synthesized and the adsorbentproperties of Ch-B composite beads were investigated for the removal/recoveryof Pb^{2+} ions in wastewater.

Materials and Methods

Chemicals and Apparatus

In this study, Na-bentonite was achieved from Merck (Germany). Medium molecular weight Ch was used (Sigma-Aldrich, Germany), $Pb(NO_3)_2$, and other chemicals were achieved from Merck (Germany) and 4-(2-pyridylazo) resorcinol (PAR) was achieved from Merck (Germany). Sodium tripolyphosphate (NaTPP), epichlorohydrin (ECH), KNO_3, HCl, C_2H_5OH, NaOH, and other chemicals were all purchased from Sigma-Aldrich. Solutions were prepared in ultrapure water.

The Ch-B composite adsorbent and its components were characterized by FT-IR (Fourier Transform Infrared Spectroscopy; ATR, Bruker Model: Tensor II), SEM (scanning electron microscopy), and energy-dispersive X-ray spectroscopy (SEM-EDX, TESCAN MIRA3 XMU). The Pb^{2+} concentration was determined with a UV–Vis spectrophotometer (SHIMADZU, 160 A model, Japan).

Preparation of Ch-B Composite Beads

Approximately 2 g of Ch and B each, were mixed in 5% (v/v) acetic acid for 2 h at 250 rpm. ECH, 4 mL, was added and the final mixture was further stirred for 2 h at 250 rpm, and then left overnight on the bench. On the following day, the mixture was added dropwise into 0.5 mol L^{-1} NaTPP solution to mold it into beads.

The Point of Zero Charges (pzc)

To determine the point of zero charges, the technique of evaluating the change of initial and equilibrium pH values was used. Equilibrium pH was measured after adding 10 mL of 0.1 M KNO_3 solutions with pHs ranging from 1 to 14 on 100 mg adsorbents and mixing for 24 h at room temperature. The initial pH values were plotted against ΔpH to obtain pzc, the point where the initial pH is equal to the final pH.

Batch Adsorption Experiments

The batch method was used (Table 1). The adsorption procedure included 10 mL of 500 mg L^{-1} Pb^{2+} solution to 100 mg of biosorbent in 10 mL polypropylene tubes and at pH 4.5. Absorbance was read at 518.5 nm [17]. Equations 1, 2, and 3. were used to estimate Adsorption%, Q (mol kg^{-1}), and Recovery% [18].

$$Adsorption\% = \left[\frac{C_i - C_f}{C_i}\right] \times 100 \quad (1)$$

$$Q = \left[\frac{C_i - C_f}{m}\right] \times V \quad (2)$$

$$Recovery\% = \frac{Q_{des}}{Q_{ads}} \times 100 \quad (3)$$

C_i, the initial concentration of Pb^{2+} (mg L^{-1}); C_f, the remaining Pb^{2+} (mg L^{-1}); V, the solution of Pb^{2+} (L); m, the quantity of the composite (g); Q_{des}, desorbed Pb^{2+} (mol kg^{-1}); and Q_{ads}, adsorbed Pb^{2+} (mol kg^{-1}).

Table 1 Experimental conditions for adsorption

Experimental Conditions					
Aim of experiment	Solution pH	Initial Pb^{2+} conc. (mg L^{-1})	Adsorbent dosage (mg)	Contact time (min)	Temperature (°C)
Effect of pH	1.0–7.0	500	100	1440	25
Effect of concentration	4.5	50–1000	100	1440	25
Effect of time	4.5	500	300	2–1440	25
Effect of adsorbent dosage	4.5	500	10, 30, 50, 100, 200	1440	25
Effect of temperature	4.5	500	100	1440	5, 25, 40
Recovery	4.5	500	100	1440	25

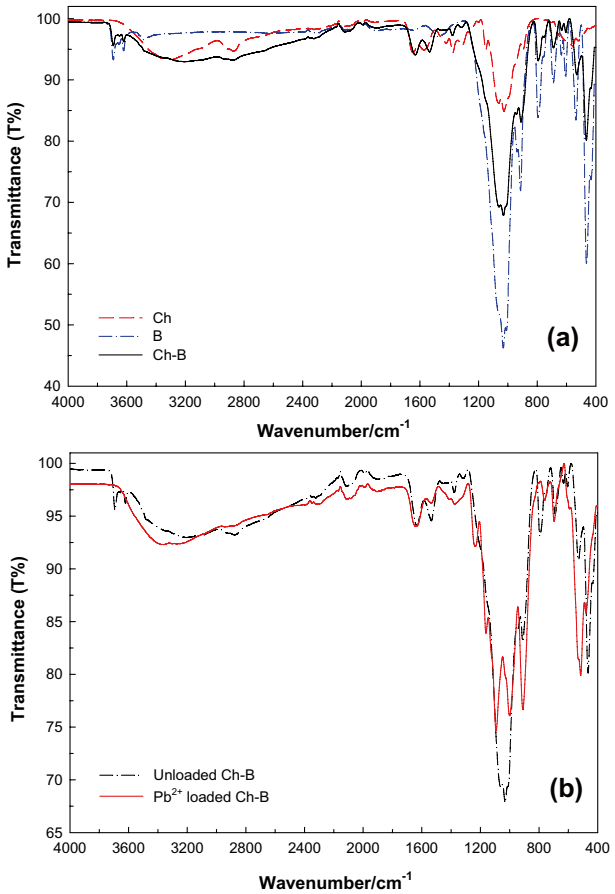

Fig. 1 FT-IR spectrum of Ch, B, Ch-B (**a**), and FT-IR spectrum of unloaded and Pb^{2+} loaded Ch-B (**b**)

Results and Discussion

FT-IR and SEM-EDX Analysis

FT-IR Spectra of Chitosan (Fig. 1a)

Characteristic peaks for chitosan; the absorption bands at 3329–3261 cm^{-1} are assigned to the NH and OH stretch, the peaks at 2941 and 2811 cm^{-1} have corresponded to the CH symmetrical and asymmetric stretching, 1645 cm^{-1} has corresponded to the C=O stretch of amide I, the 1569 cm^{-1} peak has corresponded to the NH of the primary amine, 1423 and 1375 cm^{-1} peaks are corresponded to CH_2 bending and CH_3 symmetrical deformations. The 1295 cm^{-1} peak has corresponded to the C–N stretch of amide III, the 1550 cm^{-1} peak has corresponded to the N–H bending of amide II, and the 1153 cm^{-1} peak has corresponded to the asymmetric stretch of the C–O–C bridge. The peaks at 1066–1028 cm^{-1} are assigned to the C–O stretch [19, 20].

FT-IR Spectra of Bentonite (Fig. 1a)

Characteristic peaks for bentonite; the peak at 3688 cm^{-1} was assigned to the Al–OH and Si–OH, the peak at 3619 cm^{-1} was assigned to the O–H stretching vibration, the peak at 1435 cm^{-1} was assigned to the H–O–H bending vibration, the peak at 1036 cm^{-1} was assigned to the Si–O stretching vibration, the peak at 915 cm^{-1} and 693 cm^{-1} was assigned to the Al–O stretching vibration, the peak at 794 cm^{-1} and 693 cm^{-1} was assigned to the Al–OH is the Mg–OH stretching vibration, and the Si–O groups were represented by two peaks at 533 cm^{-1} and 465 cm^{-1} [21, 22].

FT-IR Spectra of Ch-B (Fig. 1a)

In the spectrum of the Ch-B composite, the peaks at 1661 cm^{-1}, 1562 cm^{-1}, 1379 cm^{-1}, 1318 cm^{-1}, which are the functional groups of chitosan, and the peaks at 1029 cm^{-1}, 915 cm^{-1}, 792 cm^{-1}, 686 cm^{-1}, 640 cm^{-1}, 594 cm^{-1}, 526 cm^{-1} and 465 cm^{-1}, which are the functional groups of bentonite are seen. The spectrum of the Ch-B composite reveals a characteristic band at 3269 cm^{-1} which is because of hydrogen bonding formation between functional groups of Ch (N–H and O–H groups) and O–H groups in bentonite. This shows that the Ch-B composite was synthesized successfully.

FT-IR Spectra of the Pb^{2+} Loaded Ch-B (Fig. 1b)

The absorption peaks at 1562 cm^{-1} and 1661 cm^{-1} in the Ch-B composite, which shifted from 1624 to 1638 cm^{-1} in chitosan, is corresponding to the deformation vibration of amino groups. These observations confirm the participation of amine groups in the adsorption of Pb^{2+} ions to the composite surface.

SEM Images and EDX Spectra of Chitosan (Fig. 2a)

Chitosan has a fibrous, tight, scaly, and porous structure with a smooth surface [23]. The EDX spectrum of the chitosan indicated that the chitosan contained C, O, and N elements (Fig. 2a).

SEM Images and EDX Spectra of Bentonite (Fig. 2b)

Bentonite exhibits an irregular edge curve with slightly a drusy texture, partially developed crystalline laminar with a rough surface, bulk agglomerated particles and the distance between the layers was tiny [24]. The EDX spectrum of the bentonite indicated that the bentonite contained C, O, Mg, Al, Si, and Ti elements (Fig. 2b).

SEM Images and EDX Spectra of the Unloaded and Loaded Ch-B

The SEM images and EDX spectra (Fig. 2c, d) before and after Pb^{2+} ion adsorption onto Ch-B composite are presented. When the SEM images in Fig. 2c, d are examined, it is seen that the surface morphology of the Ch-B composite has changed considerably that bentonite is covered by chitosan. It is evident from the surface smoothing that Pb^{2+} ions collect on the surface of the Ch-B composite after adsorption. We believe that the observed morphology is due to surface complexation and electrostatic interactions between functional groups on the Ch-B composite surface and Pb^{2+} ions. The EDX spectrum of the Ch-B composite indicated that the Ch-B contained C, O, N,

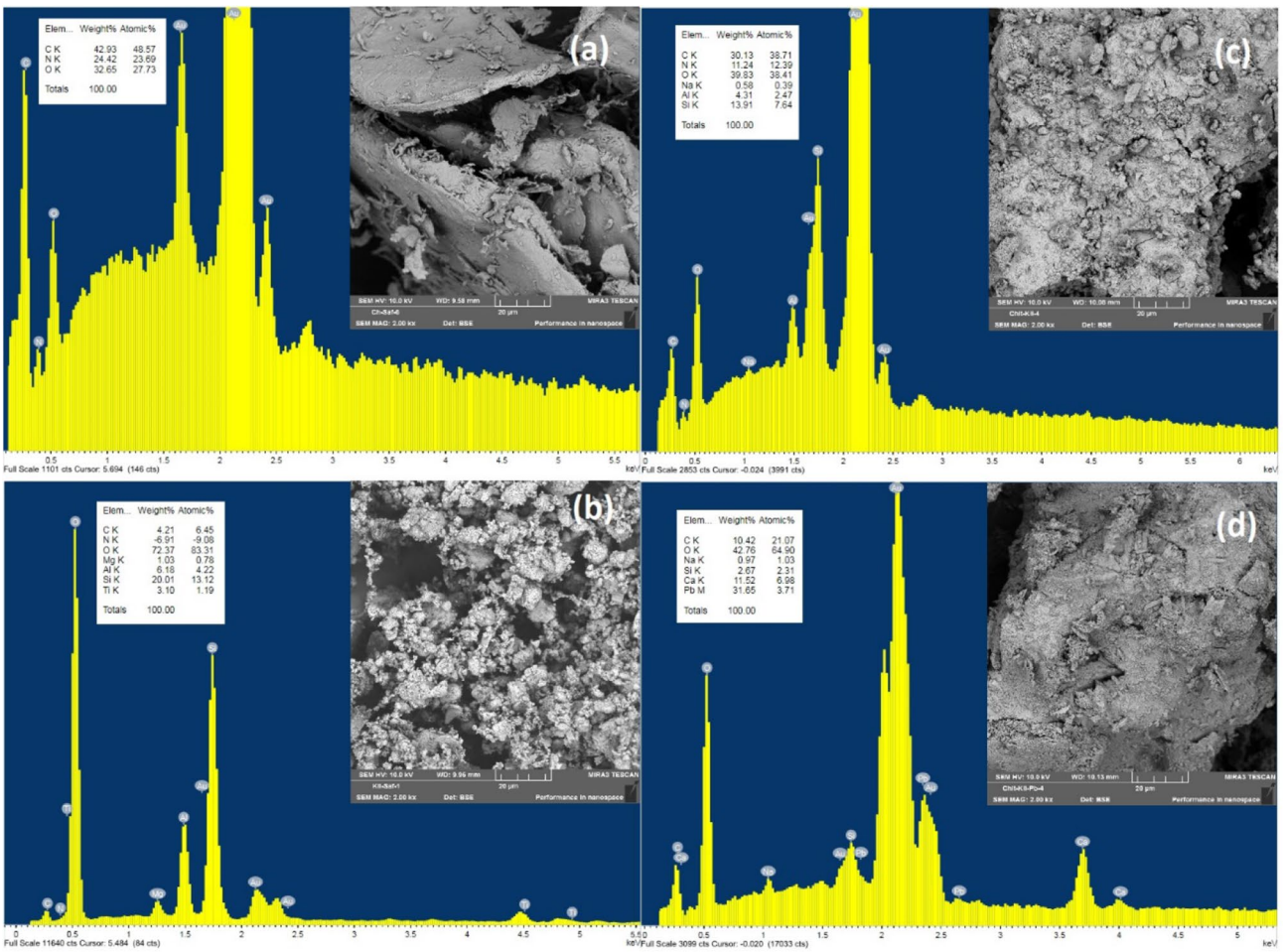

Fig. 2 SEM images and EDX spectrums Ch (**a**), B (**b**), Ch-B (**c**) and Pb^{2+} adsorption after Ch-B (**d**)

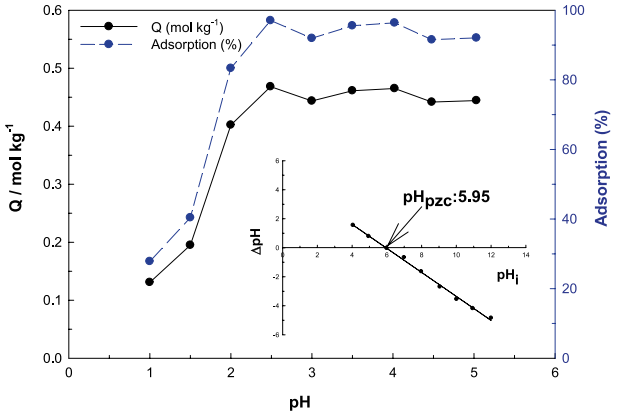

Fig. 3 Effect of pH on Pb^{2+} adsorption onto Ch-B {$[Pb^{2+}]_0$: 500 mg L^{-1}, adsorbent dosage: 100 mg, natural pH: 1.0–5.0, contact time: 24 h, temperature: 25 °C PZC for Ch-B}

Na, Al, and Si elements (Fig. 2c). The EDX spectrum of the Pb^{2+} loaded Ch-B composite showed that Pb^{2+} loaded the Ch-B composite included C, O, Na, Si, Al, and Pb (Fig. 2d). It also showed the existence of Pb after adsorption.

Effect of Initial pH and pzc for Ch-B Composite

The results regarding the effect of pH on the adsorption of Pb^{2+} ions on the Ch-B composite are presented in Fig. 3. When Fig. 3 was examined, it was observed that the adsorption increased with increasing pH. According to Fig. 3, the percentage of adsorption increased from 24 to 97%, respectively, with an increase in pH value from 1.0 to 2.5. After this point, it showed a slow decrease between pH 2.5 and 5.0. The maximum removal rate was found to be 95% at pH 4.5, which was the natural pH of the Pb^{2+} solution. At basic pHs, OH^- ions compete for adsorption to the active centers of the Ch-B composite, and Pb^{2+} ions precipitate as hydroxide. Pb^{2+} is the major species at pH below 5.5 and $PbOH^+$ is dominant at pH above 5.5 [25]. In all adsorption studies, the natural pH of the Pb^{2+} ion was studied. The natural pH of Pb^{2+} ions is 4.5 at 500 mg L^{-1}.

The pzc value of the Ch-B composite was 5.95 (Fig. 3). Acidic pHs, the surface ($pH < pH_{pzc}$) of the Ch-B composite was positive. The solution was acidic and rich in hydrated H^+ ions. In this case, H^+ ions and Pb^{2+} ions competed for attachment to the functional groups on the surface of the Ch-B composite. At basic pHs, the surface ($pH > pH_{pzc}$) of the Ch-B composite became negative. The Ch-B composite, which had an overall negative surface charge, attracted the Pb^{2+} ions electrostatically. As a result, the adsorption efficiency increased.

Effect of Adsorbent Dosage

The effect of Ch-B composite dosage on Pb^{2+} removal efficiency is given in Fig. 4. It is seen from Fig. 4 that the removal efficiency increased rapidly up to 89% with the increase of Ch-B composite adsorbent dosage by 10 g L^{-1} in 10 mL of Pb^{2+} solution, and then it remained stable by increasing a little more. As the adsorbent dosage increases, the removal of Pb^{2+} ions increases. When all surfaces are filled with Pb^{2+} ions, the adsorption came to equilibrium. Contrary to the increase in the adsorption efficiency, the adsorption capacity values decreased with the increase of the adsorbent dosage. The amount of Pb^{2+} ion retained per unit adsorbent decreased. When these two findings were evaluated together, it was determined that a 10 g L^{-1} adsorbent dosage was the most appropriate value.

Modeling of Adsorption Process

Adsorption isotherms are graphs expressing the equilibrium state between the amount of substance adsorbed on the adsorbent and the remaining substance concentration in the equilibrium solution at constant temperature and pH. These graphs are obtained by equilibration of solutions prepared at different concentrations with a certain amount of adsorbent at constant temperature and pH. Three adsorption isotherm models are commonly used. These are the Langmuir, Freundlich and Dubinin–Radushkevich (D-R) isotherm models (Table 2). The Langmuir isotherm model assumes that adsorption takes place on a homogeneous surface. It accepts that the active centers on this surface have the same energy and equal affinity towards the substance to be adsorbed. It also assumes that adsorption takes place in a monolayer [26, 27]. The Freundlich isotherm model assumes that the adsorbent

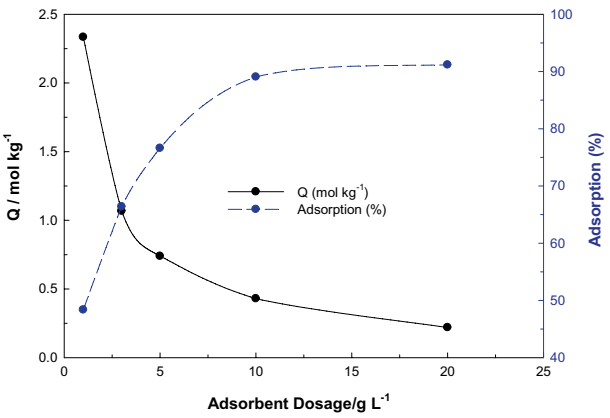

Fig. 4 Effect of adsorbent dosage on Pb^{2+} adsorption onto Ch-B {$[Pb^{2+}]_0$: 500 mg L^{-1}, adsorbent dosage: 10, 30, 50, 100 and 200 mg, natural pH: 4.5, contact time: 24 h, temperature: 25 °C}

Table 2 Adsorption isotherms and their parameters

Isotherm models	Equation	Parameters
Langmuir	$Q = \frac{X_L K_L C_e}{1+K_L C_e}$	X_L: the maximum adsorption capacity K_L: the parameter for Langmuir isotherm Q: the amount of adsorbed Pb^{2+} C_e: the equilibrium concentration
Parameter	Value	R^2
X_L (mol kg^{-1})	0.425	0.911
K_L (L mol^{-1})	4431	
Freundlich	$Q = K_F C_e^{\beta}$	K_F: Freundlich constant β: adsorbent surface heterogeneity
Parameter	Value	R^2
X_F	3.65	0.809
β	0.357	
D-R	$Q = X_{DR} e^{-K_{DR}\epsilon^2}$ $\epsilon = RTln(1+\frac{1}{C_e 0.5})$ $E_{DR} = (2K_{DR})^{}$	X_{DR}: a measure of adsorption capacity K_{DR}: the activity coefficient ε: the Polanyi potential R: the ideal gas constant (8.314 $Jmol^{-1}$ K^{-1}) E_{DR}: the adsorption energy T: the absolute temperature
Parameter	Value	R^2
X_{DR} (mol kg^{-1})	1.17	0.940
$-K_{DR}x10^9/mol^2$ K J^{-2}	2.13	
E_{DR}/kJ mol^{-1}	10.5	

surface is heterogeneous in terms of adsorption areas and adsorption energy. It also assumes that the adsorption is multilayered [28, 29]. The D-R isotherm model evaluates adsorption from an energetic point of view [30, 31]. If the adsorption free energy value is 8–16 kJ mol^{-1}, the adsorption process is chemical, if E_{DR}<8 kJ mol^{-1}, the adsorption process is physical.

Experimental data were analysed by Langmuir, Freundlich and D-R isotherm models (Fig. 5; Table 2). When the R^2 values calculated from the Langmuir and Freundlich isotherm models were compared, it was seen that the adsorption process fitted better in the Langmuir isotherm model. The monolayer adsorption capacity was found to be 0.425 mol kg^{-1}. In Langmuir constant was 4431 L mol^{-1}. The Freundlich adsorption capacity, X_F, was found to be 3.65, and the β surface heterogeneity was 0.357. The energy of the Pb^{2+} ion adsorption was calculated to be 10.5 kJ mol^{-1}. This finding indicated that the adsorption process of the Pb^{2+} ion was chemisorption.

Pb^{2+} ions adsorption capacities of various adsorbents were compared (Table 3) and the adsorption capacity of the admass of Ch-B composite was found (0.425 mol kg^{-1}). This adsorption advantage might have been derived from the richness of the functional groups on the Ch-B composite surface. Therefore, the use of Ch-B composite as an adsorbent is an economical initiative that is needed for wastewater treatment processes due to its low cost, environmentally friendly, easy and economical preparation, and inexpensive adsorbent.

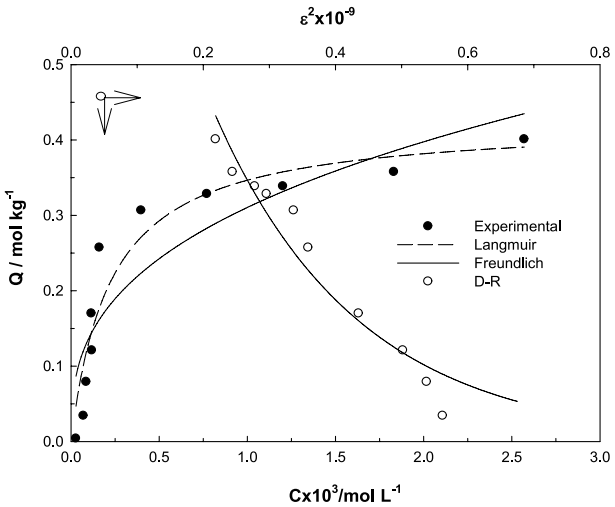

Fig. 5 Experimentally obtained adsorption isotherms Pb^{2+} onto Ch-B and their compatibility to Langmuir, Freundlich, and D-R models {$[Pb^{2+}]_0$: 50–1000 mg L^{-1}, adsorbent dosage: 100 mg, natural pH: 4.5, contact time: 24 h, temperature: 25 °C}

Table 3 Comparison of sorption capacities of other sorbents for Pb^{2+} removal

Adsorbent type	pH	Temperature (°C)	Q_{max} (mol kg^{-1})	References
Silica nanopowders/alginate	5.0	–	0.402	[32]
Magnetic chitosan/graphene oxide	5.0	30	0.372	[33]
Pinecone activated carbon	–	25	0.132	[34]
Calcium alginate beads	–	23	0.280	[35]
Amino functionalized silica gel	4.5	25	0.129	[36]
Magnetic chitosan-palygorskite	4.0	25	0.283	[37]
Chitosan-sepiolite	4.5	25	0.220	[38]
Magnetic alginate beads	–	30	0.242	[39]
Clay/poly(methoxyethyl)acrylamide	5.0	20	0.391	[40]
MoS_2-clinoptilolite	6.0	25	0.0167	[41]
Sugarcane bagasse/multi-walled carbon nanotube	4.5	28	0.273	[42]
Magnetic chitosan/graphene oxide	–	30	0.372	[33]
Epichlorohydrin-crosslinked chitosan	6.0	25	0.165	[43]
Chitosan-GLA beads	4.5	–	0.0688	[44]
Multiwalled carbon nanotubes/polyacrylamide	5.0	20	0.181	[45]
Chitosan-dolomite composite	4.0	25	0.332	[46]
Xanthate-modified magnetic chitosan	–	–	0.370	[47]
Chitosan/cellulose	5.3	25	0.130	[48]
Chitosan/hydroxyapatite	–	30	0.060	[49]
Chitosan saturated montmorillonite	5.0	–	0.238	[50]
Sodium tetraborate-modified kaolinite clay	–	28	0.207	[51]
Activated carbon prepared from *Phaseolus aureus* hulls	6.0	30	0.102	[52]
Ca(II) imprinted chitosan	–	25	0.228	[53]
Chitosan-MAA nanoparticles	5.0	–	0.0546	[54]
Chitosan-bentonite	4.5	25	0.425	This study

Effect of Contact Time on Adsorption

Adsorption kinetics is very important in terms of giving information about the mechanism of interaction between the adsorbent-adsorbate and the adsorption process. For this purpose, three types of kinetic models are commonly used, pseudo first-order (PFO) [55], pseudo-second-order (PSO) [56], and intraparticle diffusion (IPD) [57] (Table 3).

The fit of the experimental data to the PFO, PSO, and IPD models is presented in Fig. 6 and the kinetic parameters derived from these models are presented in Table 4. It was observed that the adsorption of Pb^{2+} ions reached equilibrium within 240 min (4 h) (Fig. 6). When the correlation coefficients (R^2) of the PFO and PSO models were compared with each other, it was seen that the results fit the PSO kinetic model better. In addition, the closeness of the theoretically calculated Q_t and experimental Q_e values showed compatibility with the PSO model. The appearance of two-line components instead of a single line passing through the origin in the IPD model graph indicates that adsorption includes different diffusion stages that take place both on the surface and inside the surface. In this case, it was shown that it is not possible to explain the adsorption with a single

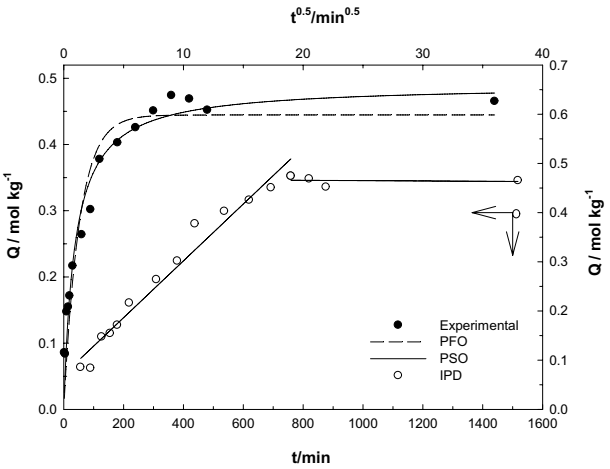

Fig. 6 Compatibility of Pb^{2+} adsorption kinetics to PFO, PSO and IPD models {$[Pb^{2+}]_0$: 500 mg L^{-1}, adsorbent dosage: 300 mg, natural pH: 4.5, contact time: 10–1440 min, temperature: 25 °C}

kinetic model. By applying experimental data to kinetic models, it was found that Pb^{2+} adsorption to Ch-B composite followed PSO and IPD kinetics. In the first stage of adsorption, there are many active centers for the adsorbent. After a

Table 4 The adsorption kinetics and their parameters

Kinetic models	Equation	Parameters
PFO	$Q_t = Q_e\left[1 - e^{-k_1 t}\right]$ $H_1 = k_1 Q_e$	Q_t: the adsorbed amount at the time Q_e: the adsorbed amount at equilibrium t: time k_1: the rate constant of the PFO H_1: initial adsorption rate for PFO
Parameter	Value	R^2
Q_t/mol kg^{-1}	0.475	0.926
Q_e/mol kg^{-1}	0.445	
$k_1 \times 10^3$/ mol^{-1} kg min^{-1}	19.1	
Hx10^3/mol kg^{-1} min^{-1}	8.50	
PSO	$Q_t = \frac{t}{\left[\frac{1}{k_2 Q_e^2}\right] + \left[\frac{t}{Q_e}\right]}$ $H_2 = k_2 Q_e^2$	k_2: the rate constant of the PSO model H_2: initial adsorption rate for PSO
Parameter	Value	R^2
Q_t/mol kg^{-1}	0.475	0.964
Q_e/mol kg^{-1}	0.490	
$k_2 \times 10^3$/mol^{-1} kg min^{-1}	55.6	
H$\times 10^3$/mol kg^{-1} min^{-1}	27.2	
IPD	$Q_t = k_i t^{0.5}$	k_i: the rate constant of the IPD
Parameter	Value	R^2
k_i x10^3/mol kg^{-1} min$^{-0.5}$	70.9	0.968

while, the number of active centers on the adsorbent surface decreases, and repulsion forces between H^+ ions and Pb^{2+} ions make it difficult to fill the active centers on the adsorbent surface. In the first stage of adsorption, it is saturated with Pb^{2+} ions. After that, Pb^{2+} ions are slowly absorbed into the pores of the adsorbent. Therefore, the adsorption slows down. In this case, it shows that the adsorption process takes place in one or more stages. The adsorption process is accompanied by surface diffusion, pore diffusion, film diffusion, diffusion on the pore surface, or more of these steps.

Effect of Temperature

The effect of temperature on the adsorption process was studied at three different temperatures, 5 °C, 25 °C, and 40 °C. The thermodynamic parameters [58, 59] for Pb^{2+} ion adsorption to Ch-B composite adsorbent, namely free Gibbs energy (ΔG^0), enthalpy (ΔH^0), and entropy (ΔS^0) of adsorption can be evaluated using the equations given (Fig. 7; Table 5). The ΔH^0 value was found to be 106 kJ mol^{-1}. This showed that the adsorption was endothermic. ΔS^0 was found to be 423 J mol^{-1} K^{-1} and showed an increase in randomness at the adsorbent/solution interface during the adsorption process. The ΔG^0 values were − 11.2 kJ mol^{-1}, − 19.5 kJ mol^{-1}, − 25.9 kJ mol^{-1} at 5 °C, 25 °C, and 40 °C, respectively. The decrease in ΔG^0 value with increases in the temperature showed that the adsorption of Pb^{2+} ions onto Ch-B composite was feasible, efficient, and spontaneous at elevated temperatures. Thermodynamic data also suggested that the Pb^{2+} ions adsorption onto Ch-B composite adsorbent was spontaneous, endothermic, and increased with entropy.

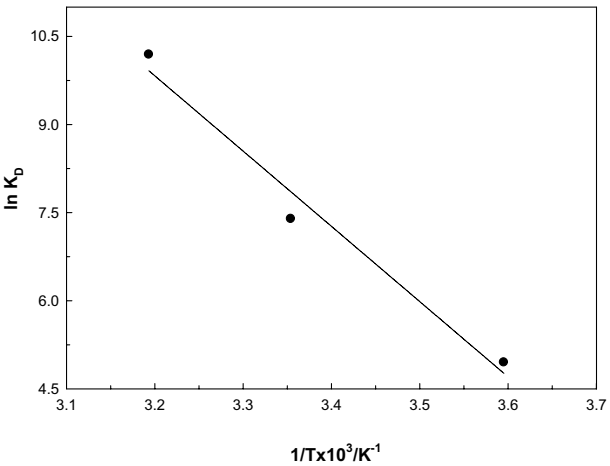

Fig. 7 The effect of temperature on the adsorption {$[Pb^{2+}]_0$: 500 mg L^{-1}, adsorbent dosage: 100 mg, natural pH: 4.5, contact time: 24 h, temperature: 5 °C, 25 °C and 40 °C}

Table 5 Adsorption thermodynamics and their parameters

Thermodynamics	Equation	Parameters
The distribution coefficients	$K_D = \frac{Q}{C_e}$	K_D: the distribution coefficients
The free energy of adsorption	$\Delta G^0 = -RTlnK_D$	ΔG^0: the free energy of adsorption (kJ mol^{-1})
Van't Hoff	$lnK_D = \frac{\Delta S^0}{R} - \frac{\Delta H^0}{RT}$	ΔH^0: the value of enthalpy changes (kJ mol^{-1}) ΔS^0: the value of entropy changes (kJ mol^{-1})

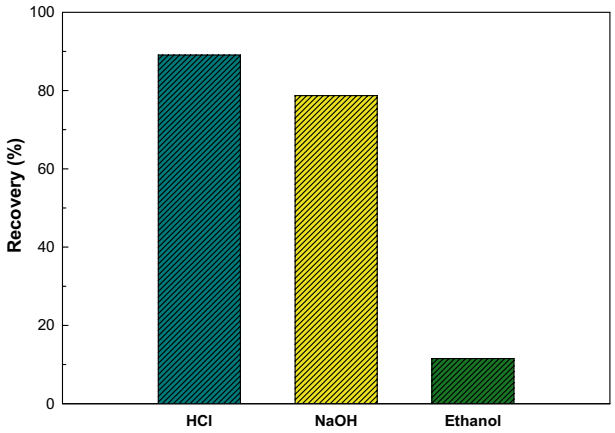

Fig. 8 The effect of recovery for Ch-B {$[Pb^{2+}]_0$: 500 mg L^{-1}, adsorbent dosage: 100 mg, natural pH: 4.5, contact time: 24 h, temperature: 25 °C}

Desorption Studies

Recovery/desorption of Pb^{2+} ions attached to the Ch-B composite surface is one of the most important stages of the adsorption process. For this purpose, three series of desorption experiments were performed with 0.1 M HCl, NaOH, HNO_3, and ethyl alcohol, and the results in Fig. 8 were obtained. As seen in Fig. 8, the highest recovery percentage for Pb^{2+} ions was obtained with HCl (84%), and the lowest recovery was obtained with ethyl alcohol (6%). This indicated that after the three recycling processes the Ch-B retained 84% of its initial adsorption capacity. And these findings were taken as proof that the Ch-B composite adsorbent could be an alternative adsorbent in the recycling of Pb^{2+} ions from industrial aqueous wastewaters.

Conclusions

In this study, the usability of Ch-B composite as an adsorbent formed for the removal of the lead ion, which is one of the common pollutants and dangerous for human health and the environment with its toxic feature, was investigated. As a result of the research, the following conclusions were reached.

(1) FT-IR and SEM images of the Ch-B composite were evaluated, and structural differences of the composite from its components were demonstrated by both analysis methods. The pzc value of the Ch-B composite was determined as 5.95.
(2) The pH effect on Pb^{2+} adsorption was investigated, and it was observed that adsorption increased with increasing pH. Adsorption experiments were performed at the natural pH of the Pb^{2+} solution.
(3) For the variation of adsorption with concentration, the compatibility of isotherms formed by adsorption study at different concentrations with commonly used adsorption models was investigated. The parameters derived from these isotherms gave information about both the properties of the adsorbent and the adsorption process.
(4) To understand the variation of adsorption over time, adsorption data were measured time and its compatibility with various kinetic models was investigated. The results showed that the adsorption kinetics can be explained by the PSO model. It is also effective in adsorption in intraparticle diffusion.
(5) In the light of adsorption thermodynamic parameters, it has been shown that adsorption is an endothermic process, the disorder increases during the adsorption process, and adsorption occurs spontaneously at 298 K.
(6) For the recovery of the adsorbed species and the regeneration of the adsorbent, stripping experiments were carried out with various solutions and it was shown that the highest efficiency was achieved with HCl.
(7) In the light of this information, it has been shown that the newly synthesized composite is a good adsorbent for Pb^{2+}, and it will be an economical, practical, easily synthesized adsorbent among other organic or inorganic pollutants.

Author Contributions ZMŞ: conceptualization, data curation, investigation, methodology, project administration, supervision, visualization, writing—original draft, writing—review and editing. SŞ: Conceptualization, data curation, investigation, methodology, writing—original draft, supervision, visualization, writing—original draft, writing—review and editing.

Funding The present study was partly supported by Sivas Cumhuriyet University Scientific Research Projects Commission.

Declarations

Conflict of interest The authors declare that there is no conflict of interest.

References

1. Majumdar SS, Das SK, Chakravarty R, Saha T, Bandyopadhyay TS, Guha AK (2010) A study on lead adsorption by *Mucor rouxii* biomass. Desalination 251:96–102
2. Cechinel MAP, de Souza AAU (2014) Study of lead (II) adsorption onto activated carbon originating from cow bone. J Clean Prod 65:342–349
3. Basu M, Guha AK, Ray L (2017) Adsorption of lead on cucumber peel. J Clean Prod 151:603–615
4. Nordberg GF, Fowler BA, Nordberg M (eds) (2014) Handbook on the toxicology of metals. Academic Press, Cambridge
5. Kumar A, MMS CP, Chaturvedi AK, Shabnam AA, Subrahmanyam G, Mondal R, Yadav KK (2020) Lead toxicity: health hazards influence on the food chain and sustainable remediation approaches. Int J Environ Res Public Health 17:2179
6. Feng Q, Lin Q, Gong F, Sugita S, Shoya M (2004) Adsorption of lead and mercury by rice husk ash. J Colloid Interface Sci 278:1–8
7. Şenol ZM, Gürsoy N, Şimşek S, Özer A, Karakuş N (2020) Removal of food dyes from aqueous solution by chitosan-vermiculite beads. Int J Biol Macromol 148:635–646
8. Şenol ZM, Gül ÜD, Gurbanov R, Şimşek S (2021) Optimization the removal of leading by fungi: explanation of the mycosorption mechanism. J Environ Chem Eng 9:104760
9. Zhang J, Shao J, Jin Q, Zhang X, Yang H, Chen Y, Chen H (2020) Effect of deashing on activation process and lead adsorption capacities of sludge-based biochar. Sci Total Environ 716:137016
10. Elsayed NH, Alatawi RA, Monier M (2021) Amidoxime modified chitosan-based ion-imprinted polymer for selective removal of uranyl ions. Carbohydr Polym 256:117509
11. Elsayed NH, Alatawi A, Monier M (2020) Diacetylmonoxine modified chitosan derived ion-imprinted polymer for selective solid-phase extraction of nickel (II) ions. React Funct Polym 151:104570
12. Lewandowska K, Sionkowska A, Kaczmarek B, Furtos G (2014) Characterization of chitosan composites with various clays. Int J Biol Macromol 65:534–541
13. Monier M, Abdel-Latif DA, Abou El-Reash YG (2016) Ion-imprinted modified chitosan resin for selective removal of Pd (II) ions. J Colloid Interface Sci 469:344–354
14. Elsayed NH, Monier M, Alatawi RA, Albalawi MA, Alhawiti AS (2022) Preparation of chromium (III) ion-imprinted polymer based on azo dye functionalized chitosan. Carbohydr Polym. https://doi.org/10.1016/j.carbpol.2022.119139
15. Monier M, Abdel-Latif DA (2017) Fabrication of Au (III) ion-imprinted polymer based on thiol-modified chitosan. Int J Biol Macromol 105:777–787
16. Banat FA, Al-Bashir B, Al-Asheh S, Hayajneh O (2000) Adsorption of phenol by bentonite. Environ Pollut 107:391–398
17. Şenol ZM, Şimşek S (2020) Equilibrium kinetics and thermodynamics of Pb (II) ions from aqueous solution by adsorption onto chitosan-dolomite composite beads. J Environ Anal Chem. https://doi.org/10.1080/03067319.2020.1790546
18. Kumar A, Patra C, Kumar S, Narayanasamy S (2022) Effect of magnetization on the adsorptive removal of emerging contaminant ciprofloxacin by magnetic acid activated carbon. Environ Res 206:112604
19. Pawlak A, Mucha M (2003) Thermogravimetric and FTIR studies of chitosan blends. Thermochim Acta 396:153–166
20. Ren L, Xu J, Zhang Y, Zhou J, Chen D, Chang Z (2019) Preparation and characterization of porous chitosan microspheres and adsorption performance for hexavalent chromium. Int J Biol Macromol 135:898–906
21. Kumar A, Lingfa P (2020) Sodium bentonite and kaolin clays: comparative study on their FT-IR XRF and XRD. Mater Today: Proc 22:737–742
22. Ren Y, Wang H, Ren Z, Zhang Y, Geng Y, Wu L, Pu X (2019) Adsorption of imidazolium-based ionic liquid on sodium bentonite and its effects on rheological and swelling behaviors. Appl Clay Sci 182:105248
23. Hassan AF, Hrdina R (2018) Chitosan/nanohydroxyapatite composite based scallop shells as an efficient adsorbent for mercuric ions: Static and dynamic adsorption studies. Int J Biol Macromol 109:507–516
24. Niu M, Li G, Cao L, Wang X, Wang W (2020) Preparation of sulfate aluminate cement amended bentonite and its use in heavy metal adsorption. J Clean Prod 256:120700
25. Kovačević D, Pohlmeier A, Özbaş G, Narres HD, Kallay MJN (2000) The adsorption of lead species on goethite. Colloids Surf A Physicochem Eng 166:225–233
26. Langmuir I (1918) The adsorption of gases on plane surfaces of glass mica and platinum. J Am Chem Soc 40:1361e1403
27. Priyan VV, Kumar N, Narayanasamy S (2021) Development of Fe3O4/CAC nanocomposite for the effective removal of contaminants of emerging concerns (Ce3+) from water: an ecotoxicological assessment. Environ Pollut 285:117326
28. Freundlich HMF (1906) Over the adsorption in solution. J Phys Chem A 57:385–471
29. Shahnaz T, Patra C, Sharma V, Selvaraju N (2020) A comparative study of raw, acid-modified, and EDTA-complexed *Acacia auriculiformis* biomass for the removal of hexavalent chromium. Chem Ecol 36(4):360–381
30. Dubinin MM, Zaverina ED, Radushkevich LV (1947) Sorption and structure of active carbons I. Adsorption of organic vapors. Zh Fiz Khim 21:1351–1362
31. Kumar N, Narayanasamy S (2022) Toxicological assessment and adsorptive removal of lead (Pb) and Congo red (CR) from water by synthesized iron oxide/activated carbon (Fe3O4/AC) nanocomposite. Chemosphere 294:133758
32. Soltani RDC, Khorramabadi GS, Khataee AR, Jorfi S (2014) Silica nanopowders/alginate composite for adsorption of lead (II) ions in aqueous solutions. J Taiwan Inst Chem Eng 45(3):973–980
33. Fan L, Luo C, Sun M, Li X, Qiu H (2013) Highly selective adsorption of lead ions by water-dispersible magnetic chitosan/graphene oxide composites. Colloids Surf B 103:523–529
34. Momčilović M, Purenović M, Bojić A, Zarubica A, Ranđelović M (2011) Removal of lead (II) ions from aqueous solutions by adsorption onto pine cone activated carbon. Desalination 276(1–3):53–59
35. Mata YN, Blázquez ML, Ballester A, González F (2009) Muñoz ICrption of cadmium, lead and copper with calcium alginate xerogels and immobilized Fucus vesiculosus. J Hazard Mater 163:555–562
36. Najafi M, Yousefi Y (2012) Rafati Synthesis, characterization and adsorption studies of several heavy metal ions on amino-functionalized silica nano hollow sphere and silica gel. Sep Purif Technol 85:193–205
37. Rusmin R, Sarkar B, Mukhopadhyay R, Tsuzuki T, Liu Y, Naidu R (2022) Facile one-pot preparation of magnetic

chitosan-palygorskite nanocomposite for efficient removal of lead from water. J Colloid Interface Sci 608:575–587
38. Senol-Arslan D (2021) Isotherms, kinetics, and thermodynamics of Pb (II) adsorption by crosslinked chitosan/sepiolite composite. Polym Bull. https://doi.org/10.1007/s00289-021-03688-9
39. Idris A, Ismail NSM, Hassan N, Misran E (2012) Ngomsik Synthesis of magnetic alginate beads based on maghemite nanoparticles for Pb(II) removal in aqueous solution J. Ind Eng Chem 18:1582–1589
40. Şölener M, Tunali S, Özcan AS, Özcan A, Gedikbey T (2008) Adsorption characteristics of lead (II) ions onto the clay/poly (methoxyethyl) acrylamide (PMEA) composite from aqueous solutions. Desalination 223(1–3):308–322
41. Pandey S, Fosso-Kankeu E, Spiro MJ, Waanders F, Kumar N, Ray SS et al (2020) Equilibrium, kinetic, and thermodynamicstudies of lead ion adsorption from mine wastewater onto MoS2-clinoptilolitecomposite. Mater Today Chem 18:100376
42. Hamza IA, Martincigh BS, Ngila JC, Nyamori VO (2013) Adsorption studies of aqueous Pb (II) onto a sugarcanebagasse/multiwalled carbon nanotube composite. Phys Chem Earth A/b/c 66:157–166
43. Chen AH, Liu SC, Chen CY, Chen CY (2008) Comparative adsorption of Cu (II), Zn (II), and Pb (II) ions in aqueous solution on the crosslinked chitosan with epichlorohydrin. J Hazard Mater 154(1–3):184–191
44. Wan Ngah WS (2010) Fatinathan Pb (II) biosorption using chitosan and chitosan derivatives beads: equilibrium, ion exchange and mechanism studies. J Environ Sci 22(3):338–346
45. Yang S, Hu J, Chen C, Shao D, Wang X (2011) Mutual effects of Pb (II) and humic acid adsorption on multiwalled carbon nanotubes/polyacrylamide composites from aqueous solutions. Environ Sci Technol 45(8):3621–3627
46. Şenol ZM, Şimşek S (2020) Equilibrium, kinetics, and thermodynamics of Pb (II) ions from aqueous solution by adsorption onto chitosan-dolomite composite beads. Int J Environ Anal Chem. https://doi.org/10.1080/03067319.2020.1790546
47. Zhu Y, Hu J, Wang J (2012) Competitive adsorption of Pb (II), Cu (II), and Zn (II) onto xanthate-modified magnetic chitosan. J Hazard Mater 221:155–161
48. Sun X, Peng B, Ji Y, Chen J, Li D (2009) Chitosan (chitin)/cellulose composite bio sorbents prepared using ionic liquid for heavy metal ions adsorption. AIChE J 55(8):2062–2069
49. Gupta N, Kushwaha AK, Chattopadhyaya MC (2012) Adsorptive removal of Pb^{2+}, Co^{2+}, and Ni^{2+} by hydroxyapatite/chitosan composite from aqueous solution. J Taiwan Inst Chem Eng 43:125–131
50. Hu C, Zhu P, Cai M, Hu H, Fu Q (2017) Comparative adsorption of Pb (II), Cu (II), and Cd (II) on chitosan saturated montmorillonite: kinetic, thermodynamic, and equilibrium studies. Appl Clay Sci 143:320–326
51. Unuabonah EI, Adebowale KO, Olu-Owolabi BI, Yang LZ, Kon LX (2008) Adsorption of Pb(II) and Cd(II) from aqueous solutions onto sodiumtetraborate-modified kaolinite clay: equilibrium and thermodynamic studies. Hydrometallurgy 93:1–9
52. Rao MM, Ramana DK, Seshaiah K, Wang MC (2009) Chang removal of some metal ions by activated carbon prepared from Phaseolus aureus hulls. J Hazard Mater 166:1006–1013
53. He J, Lu Y (2014) Luo Ca(II) imprinted chitosan microspheres: an effective and green adsorbent for the removal of Cu(II), Cd(II), and Pb(II) from aqueous solutions. Chem Eng J 244:202–208
54. Heidari A, Younesi H, Mehraban Z (2013) Heikkinen Selective adsorption of Pb(II), Cd(II), and Ni(II) ions from aqueous solution using chitosan–MAA nanoparticles. Int J Biol Macromol 61:251–263
55. Ho YS, McKay G (1998) Kinetic models for the sorption of dye from aqueous solution by wood. J Environ Sci Health B 76:183–191
56. Ho YS, McKay G (1999) Pseudo-second order model for sorption processes. Process Biochem 34:451–465
57. Weber WJ, Morris JC (1963) Kinetics of adsorption on carbon from solution. Publ Pa Div Sanit Eng 89:31–60
58. Lima EC, Hosseini-Bandegharaei A, Moreno-Piraján JC, Anastopoulos I (2019) A critical review of the estimation of the thermodynamic parameters on adsorption equilibria. Wrong use of equilibrium constant in the Van't Hoof equation for calculation of thermodynamic parameters of adsorption. J Mol Liq 273:425–434
59. Shahnaz T, Priyan VV, Jayakumar A, Narayanasamy S (2022) Magnetic nanocellulose from *Cyperus rotundas* grass in the absorptive removal of rare earth element cerium (III): toxicity studies and interpretation. Chemosphere 287:1319